Multiband Analysis of Photoluminescence Spectra from Electronically Excited Gas-Phase Species Produced during Laser Ablation of Lead Oxide, Zirconium Oxide, Titanium Oxide, and Lead Zirconate Titanate Targets

N. R. Barnes,[†] R. Dat,[‡] D. J. Lichtenwalner,[‡] A. F. Schreiner,*[,†] O. Auciello,[‡,⊥] and O. E. Hankins[§]

Departments of Chemistry, Materials Science and Engineering, and Nuclear Engineering, North Carolina State University, Raleigh, North Carolina 27695, and MCNC, Electronics Technology Division, Research Triangle Park, North Carolina 27709-2889

Received June 14, 1994. Revised Manuscript Received December 19, 1994[⊗]

The analysis of multiband/line photoluminescence spectra produced by electronically excited gas-phase species in the plasma plume, generated by impact of a KrF excimer laser beam (248 nm) on various metal oxide targets, has been carried out, and the results are reported here. It was established that, at 1.1 J/cm^2 in 900 mTorr of O_2, (i) Pb(I), Pb(II), and O_2^+ are generated from PbO(s) targets; (ii) Zr(I), Zr(II), ZrO, O_2, and O_2^+ from ZrO_2(s) targets; (iii) Ti(I), Ti(II), TiO, TiO_2, and O_2^+ from TiO_2(s) targets; and (iv) Pb(I), Pb(II), PbO, Zr(I), Zr(II), ZrO, Ti(I), Ti(II), TiO, TiO_2, O(I), O(II), O_2, and O_2^+ from a solid $Pb(Zr_xTi_{1-x})O_3$(PZT) target. The observation of excited oxygen species may be attributed to the presence of ambient molecular O_2 and/or the oxygen-rich metal oxide and PZT targets. The much lower standard enthalpy of atomization, $\Delta H°_a$, for PbO(s) and the much higher $\Delta H°_a$ values for ZrO_2(s) and TiO_2(s) are consistent with observing molecular metal oxide species, MO_n(g), in the ablation plume from ZrO_2(s) and TiO_2(s) but observing almost exclusively atomic Pb(I) and Pb(II) from the PbO(s) target. Additionally, a detailed explanation regarding the observation of lower-charged atomic metal species and not the higher-charged (formally ionic) species is presented. Particle ejection is briefly discussed as also is the relative influence of the observed species on thin-film deposition.

Introduction

Pulsed laser ablation-deposition (PLAD), involving the thin-layer ablation from a solid bulk target by singly or multiply pulsed (excimer) laser irradiation of a target area, results in subsequent film deposition on a suitable substrate. It is a relatively simple method for producing high-quality thin films of single or complex, multicomponent materials. Some of the other current successful methods, to mention a few, include sputtering,[1-3] thermal and electron beam evaporation,[4-7] sol–gel,[8,9] molecular beam deposition,[10] MOCVD, and atomic layer epitaxy. The PLAD technique has a number of good features: it is relatively inexpensive, it produces excellent transfer of stoichiometry from target to film for many systems (e.g., YBCO), it can produce crystalline growth at relatively low substrate temperatures (≤650 °C), it may be used in the analysis of solid samples without initial chemical preparation, and it has the potential of making possible the analysis of very small microstructures when the laser beam is focused by a high-quality lens and the beam wavelength is short. The PLAD technique has been used to produce films of superconductors, semiconductors, insulators, and some metallic materials.[11]

For the above-mentioned reasons, PLAD has rapidly emerged as a scientifically important and useful method for exploring the synthesis of new thin-film materials—as, for example, thin films of high-T_c (T_c = 90–93 K) superconductors from the ablation of bulk $YBa_2Cu_3O_{7-\delta}$ (YBCO) targets. Such as-deposited high-T_c films have been produced containing excellent crystallinity and other properties.[11] In fact, the majority of PLAD studies to date have concentrated on the ablation of YBCO. The success achieved in synthesizing YBCO films has also

[†] Department of Chemistry.
[‡] Department of Materials Science and Engineering.
[§] Department of Nuclear Engineering.
[⊥] MCNC, Electronics Technology Division.
* To whom correspondence should be addressed.
[⊗] Abstract published in *Advance ACS Abstracts,* February 1, 1995.

(1) Enomoto, Y.; Murakami, T.; Suzuki, M.; Moriwaki, K. *Jpn. J. Appl. Phys.* **1987**, *26*, L1248.
(2) Char, K.; Kent, A. D.; Kapitulnik, A.; Beasley, M.•R.; Geballe, T. H. *Appl. Phys. Lett.* **1987**, *51*, 1370.
(3) Li, H. C.; Linker, G.; Ratzel, F.; Smithey, R.; Geerk, J. *Appl. Phys. Lett.* **1988**, *52*, 1098.
(4) Laibowitz, R. B.; Koch, R. H.; Chandhari, P.; Gambino, R. J. *Phys. Rev. B* **1987**, *35*, 8821.
(5) Mankilwich, P. M.; Scofield, J. H.; Skocpol, W. J.; Howard, R. E.; Dayem, A. H.; Good, E. *Appl. Phys. Lett.* **1987**, *51*, 1753.
(6) Naito, M.; Hammond, R. H.; Oh, B.; Hahn, M.; Hsu, J. W. P.; Rosenthal, P.; Marshall, A.; Beasley, M. R.; Kapitulnik, A.; Geballe, T. H. *J. Mater. Res.* **1987**, *2*, 713.
(7) Lathrop, D. K.; Russek, S. E.; Buhrman, R. A. *Appl. Phys. Lett.* **1987**, *51*, 1554.
(8) Kwo, J.; Hsieh, T. C.; Fleming, R. H.; Hong, M.; Lion, S. H.; Davidson, B. A.; Feldman, L. C. *Phys. Rev. B* **1987**, *36*, 4089.
(9) Webb, C.; Weng, S.-L.; Eckstein, J. N.; Missert, N.; Char, K.; Schlom, D. G.; Hellman, E. S.; Beasley, M. R.; Kapitulnik, A.; Harris, Jr., J. S. *Appl. Phys. Lett.* **1987**, *51*, 1191.
(10) Rice, C. E.; van Dover, R. B.; Fisanick, G. J. *Appl. Phys. Lett.* **1987**, *51*, 1842.
(11) Auciello, O. *Mater. Manuf. Processes* **1991**, *6*, 33.

0897-4756/95/2807-0477$09.00/0

encouraged researchers to use PLAD for producing other perovskite-like thin films, which also have potential microelectronics applications. The PLAD-produced and bulk ferroelectric ceramic $PbZr_xTi_{1-x}O_3$ (PZT) is one such material now being investigated in the hope of finding future utility[12] in nonvolatile random access memories (NVRAM) and electrooptic devices. While some, but by far not full, understanding of PZT deposition by PLAD exists, there have been successes[12-15] in growing in situ thin films of this increasingly important ferroelectric material. PZT displays a large remnant polarization, P_r, which, according to recent findings, remains practically constant up to about 10^{10} switching cycles[16] for these PLAD-deposited epitaxial films of PZT on oxide electrodes such as $La_{0.5}Sr_{0.5}CoO_3$ (LSC).[16,17]

Although PZT, YBCO, and LSC have similar perovskite-like structures, it must be noted that the growth of high-quality thin films of PZT, as compared to films of YBCO and LSC, is more difficult. This is mainly due to the fact that Pb and PbO are relatively quite volatile, which in turn leads to Pb and PbO loss during film growth. The control of Pb loss is important because it can result in the nucleation of an undesirable pyrochlore phase, which does not have ferroelectric properties and leads to degradation of the electrical characteristics of the PZT film. Only by careful control of the various deposition and growth parameters—in particular, ambient oxygen pressure ($p(O_2)$), substrate temperature (T_s), target–substrate distance (D_{t-s}), and laser fluence (J/cm^2)—can one successfully synthesize epitaxial films of PZT, viz., those possessing correct stoichiometry, microstructure, and good surface morphology.

In a recent study[18] our group investigated the effects of laser pulse energy, ablation time, and background oxygen pressure (during ablation of PZT targets) on the three consequences of (i) angular distribution of deposited species, (ii) deposition rate, and (iii) types of electronic excited-state species in the plasma plume, species which are probably the building blocks of the thin film. In our initial optical emission spectroscopy (OES) study[18] it was found that atomic species—neutral and ionic—were present, but there was no direct evidence at that time for the existence of molecular species. Moreover, the lower spectral resolution utilized then did not accurately indicate the relative proportions of photoluminescent species. In the present study, however, we report the results and detailed analysis of the OES-detected species in the ablation plumes from PZT, PbO, ZrO_2, and TiO_2 targets using higher than our previously used spectral resolution. Major objectives of the work described in this paper were to (1) search for the presence of molecular species in the plume, (2) identify the excited species and their charges, and (3) determine factors possibly relevant to the mechanism(s) responsible for the generation of molecular species in the ablation plume.

Experimental Section

Each of four disk targets of PbO, ZrO_2, TiO_2, and PZT-[$Pb(Zr_{0.52}Ti_{0.48})O_3$ + 10%PbO] were prepared via conventional pressing and sintering techniques. Targets were irradiated by a KrF pulsed excimer laser (λ = 2480 Å, τ = 25 ns, 10 Hz repetition rate, and 400 mJ/pulse) at a 45° angle of incidence from the target normal. The laser beam was focused on each target surface using a Suprasil lens, producing a rectangular spot. Laser impact at the target yielded a plasma plume symmetrical with respect to the target normal and which projected away from the target along the target normal. A Coherent Labmaster-E meter was utilized to measure the pulse energy (0.40 J) at a position between the laser source and the target, and the focused beam area (0.18 cm^2) was determined by producing a mark on a Polaroid-type 55 negative film with one laser pulse. We find that a 50% drop in laser energy occurs by passing it through the lens and chamber window. Hence, the average laser pulse energy density is 1.1 J/cm^2.

The vacuum system employed in the ablation experiments consisted of a stainless steel chamber pumped by a 510 L/s turbomolecular pump (TPU 510) which, following the insertion of a conductance limiting aperture, allowed chamber pressures to approach 1 Torr (1.33×10^5 mPa) with the pump on. An MKS brand mass flow meter in series with a solenoid control valve was used to control oxygen gas flow, and a Granville Phillips Convectron gauge was used to monitor the chamber pressure. A load-lock chamber equipped with a magnetically coupled transfer rod enabled targets to be exchanged without breaking vacuum. A rotating target holder, designed and built by our group,[19] was used for the work described in this paper. The target holder has a capacity for holding up to six targets, each of which can sequentially be exposed to the laser beam by means of an automatically controlled rotation. The holder features a capability for continuous rotation of each target when exposed to the laser beam to minimize undesirable surface topography.

For the acquisition of photoluminescence spectra, an optical multichannel analyzer (OMA)—comprised of a computer, a grating monochromater, and a diode array detector—was employed in conjunction with a movable fiber optic conduit positioned perpendicular to the laser ablation-induced plasma. The OMA is controlled by a Tracor Northern 6500 data acquisition system. The detector is a 512-element silicon photodiode linear array (0.025 mm diode width) located at the focal plane of a 0.25 m monochromator with a 600 groove/mm diffraction grating (giving rise to a 0.15 nm sampling interval and a spectral resolution of 0.16 nm for a 75 nm dispersion window). Light generated from the optical emission of excited species within the plasma plume was collected and transmitted through a 0.4 mm diameter optical fiber positioned perpendicular to the ablation plume axis and mounted on a linear motion feedthrough at a distance of 0.5 cm from the target surface. The fiber optic was positioned inside a stainless steel tube and recessed to prevent deposition on the fiber end and to use the tube aperture as a light acceptance slit.

Spectra shown in this paper were obtained from the plasma-plume produced by the ablation of each target in vacuum ($\sim 10^{-6}$ Torr) and in a background gas (O_2) atmosphere at 300, 600, and 900 mTorr in two separate wavelength ranges, one in the ultraviolet region and the other in the visible region, viz., a 75 nm wide "blue" region (~340–415 nm) and a 75 nm wide "red" region (~555–630 nm). The spectra obtained in vacuum, 300 mTorr of O_2, and 600 mTorr of O_2 are not presented in this work, since they revealed the presence of

(12) Kodoh, H.; Ogawa, T.; Morimoto, A.; Shimizu, T. *Appl. Phys. Lett.* **1991**, *58*, 2910.
(13) Horwitz, J. S.; Grabowski, K. S.; Chrisey, D. B.; Leuchtner, R. E. *Appl. Phys. Lett.* **1991**, *59*, 1565.
(14) Chrisey, D. B.; Horwitz, J. S.; Grabowski, K. S. *Mater. Res. Soc. Symp. Proc.* **1990**, *191*, 25.
(15) Auciello, O.; Mantese, L.; Duarte, J.; Chen, X.; Rou, S. H.; Kingon, A. I.; Schreiner, A. F.; Krauss, A. R. *J. Appl. Phys.* **1993**, *73*(10), 5197.
(16) Ramesh, R.; Chan, W. K.; Wilkens, B.; Gilchrist, H.; Sands, T.; Tarascon, J. M.; Keramides, V. G.; Fork, D. K.; Lee, J.; Safari, A. *Appl. Phys. Lett.* **1992**, *61*, 1537.
(17) Lichtenwalner, D. J.; Dat, R.; Auciello, O.; Kingon, A. I. *Ferroelectrics*, in press.
(18) Lichtenwalner, D. J.; Auciello, O.; Dat, R.; Barnes, R.; Schreiner, A. F.; Hankins, O. E.; Kingon, A. I. *Ferroelectric Thin Films III*; Tuttle, B. A., Myers, E. R., Desu, S. B., Larsen, P. K., Eds.; Mat. Res. Soc. Proc.; Pittsburgh, PA, **1993**; Vol. 310, p 481.
(19) Auciello, O.; Emerick, J.; Duarte, J.; Illingworth, A. *J. Vac. Sci. Technol.* **1993**, *11*, 267.

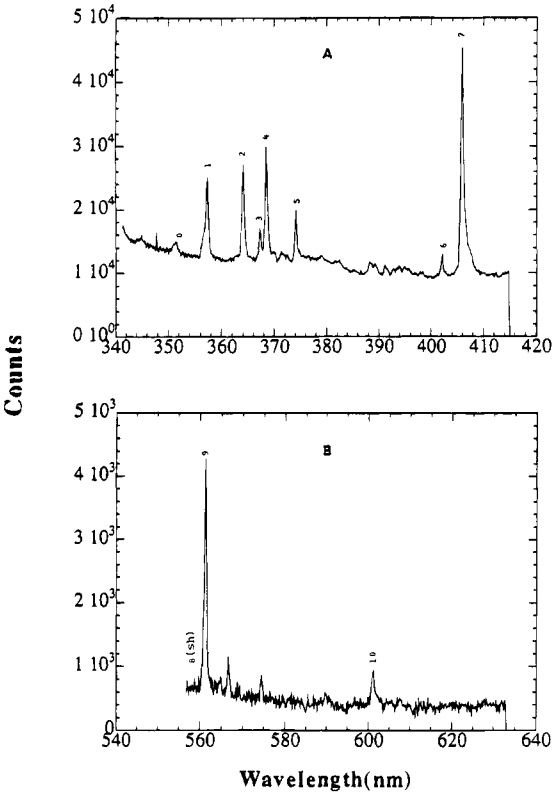

Figure 1. Relative optical emission intensity (counts) vs wavelength (nanometers) of the laser ablation plume from PbO(s) in a 900 mTorr of O_2 atmosphere. Spectra obtained in the "blue" (A) and "red" (B) regions.

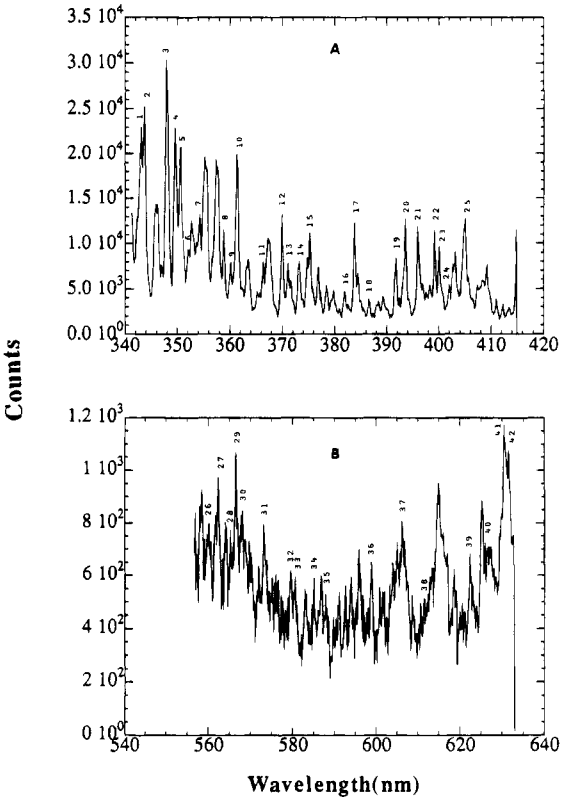

Figure 2. Relative optical emission intensity (counts) vs wavelength (nanometers) of the laser ablation plume from ZrO_2(s) in a 900 mTorr of O_2 atmosphere. Spectra obtained in the "blue" (A) and "red" (B) regions.

the same peaks as at the 900 mTorr of O_2 pressure. Also, their peak intensities were significantly less than those measured at 900 mTorr of O_2. The OMA was first calibrated with Hg (for the 320–620 nm range) and Kr (for the 530–830 nm range) pen lamps, and the spectra were directly displayed on the computer screen (peak height vs nm). A background spectrum was then collected and stored in the computer memory and automatically subtracted from each emission spectrum to correct for dark current signals produced by the photodiode array, which was held at room temperature. The emission spectra were subsequently plotted using a MacIntosh computer running Kaleidagraph software.

Results and Discussion

Optical emission spectra of the plasma plumes produced during laser ablation from solid PbO, ZrO_2, TiO_2, and $Pb(Zr_xTi_{1-x})O_3$ are shown in Figures 1–4. The emission wavelengths of peak maxima are given in the tables; they were obtained by carefully searching the digitized spectra. Following commonly used atomic spectroscopic literature[20] notation (excited-state) neutral atoms are labeled (I), while their (excited-state) ions are labeled (II), (III), etc., for charges +1, +2, etc., respectively.

We start this section with PbO(s), and Figures 1A and 1B, showing the optical emission spectra of the PbO ablation plume in a 900 mTorr of O_2 background. For the sake of definitively identifying photoluminescent elements or molecules, we label only those peaks which are clearly identifiable with just one species, and a few peaks identifiable with more than one species. Correspondingly, Tables 1 and 2 indicate by peak number,

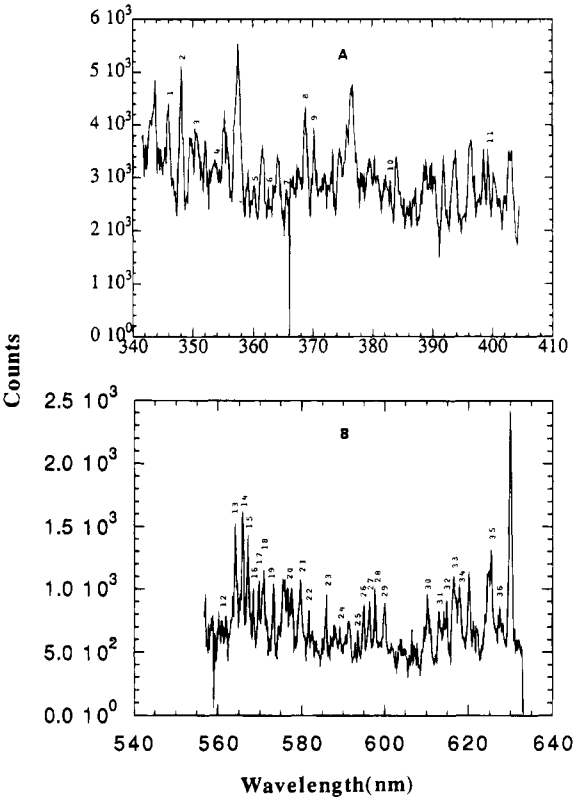

Figure 3. Relative optical emission intensity (counts) vs wavelength (nanometers) of the laser ablation plume from TiO_2(s) in a 900 mTorr of O_2 atmosphere. Spectra obtained in the "blue" (A) and "red" (B) regions.

wavelength, and species type(s) those photoluminescent chemical entities yielding the observed emission iden-

(20) Zaidel', A. N.; Prokof'ev, V. K.; Raiskii, S. M. *Tables of Spectrum Lines*; Pergamon Press: London, 1961.

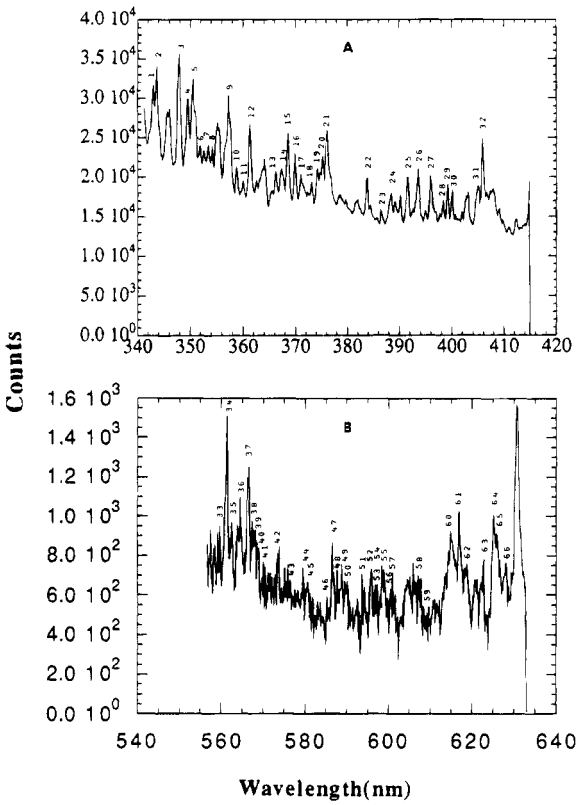

Figure 4. Relative optical emission intensity (counts) vs wavelength (nanometers) of the laser ablation plume from $PbZr_xTi_{1-x}O_3$(s) in a 900 mTorr of O_2 atmosphere. Spectra obtained in the "blue" (A) and "red" (B) regions.

Table 1. Laser Ablation of PbO (900 mTorr of O_2): Clearly Identifiable Photoluminescence Peaks of Gaseous Atomic Species Observed in the "Blue" Region (340–415 nm)

peak no.	emitting species[a]	experimental wavelengths, Å	lit.[b] wavelengths, Å	lit. ref
0	O_2^+	3517	3518	21
1	Pb(I)	3574	3573	20
2	Pb(I)	3641	3640	20
3	Pb(I)	3674	3672	20
4	Pb(I)	3685	3683	20
5	Pb(I)	3742	3740	20
6	Pb(I)[c]/O_2[d]	4021	4020,[c] 4021[d]	20,21
7	Pb(I)	4059	4058	20

[a] Excited-state neutral atoms are labeled I. [b] Emission wavelengths of arc or spark excitations. [c,d] Pb(I) and O_2 emit at 4020 and 4021 Å, respectively.

Table 2. Laser Ablation of PbO (900 mTorr of O_2): Clearly Identifiable Photoluminescence Peaks of Gaseous Atomic and Molecular Species Observed in the "Red" Region (555–630 nm)

peak no.	emitting species[a]	experimental wavelengths, Å	lit.[b] wavelengths, Å	lit. ref
8	O_2^+	5602(sh)	5598	21
9	Pb(II)[c]/PbO[d]	5613	5609,[c] 5618[d]	20, 21
10	Pb(II)	6010	6010	20

[a] Excited-state ions (+1) are labeled II. [b] Emission wavelengths of arc, spark, or discharge tube excitations. [c,d] Pb(II) and PbO emit at 5609 and 5618 Å, respectively.

tifiable from literature data.[20,21] In both spectra we observe very few peaks (with most appearing in Figure 1A), which we assign mainly to Pb(I), or Pb^0. In fact, peaks 1–5 and 7 in Figure 1A are due solely to Pb(I) atomic emission. Peak 0 is assigned to diatomic O_2^+. Peak 6 (4021 Å), on the basis of having comparable emission wavelengths, can be due to either or both atomic Pb(I) (4020 Å) and molecular O_2 (4021 Å) photoluminescence. Figure 1B displays just two peaks (9 and 10). Peak 9 (5613 Å), a very intense emission, may be attributed to both PbO and Pb(II), an assignment which is in fair agreement with the literature. Peak 10 (6010 Å) reveals the presence of weakly emitting Pb(II). It is also interesting that peak 9 has a blue shoulder (shoulder 8), the energy of which is in close agreement with the O_2^+ emission known to occur at 5598 Å (21). Such a concurrence is also there for the O_2^+ emission known at 3517 Å, with which our peak 0 nearly coincides (Table 1). Two other weak emissions are at 5665 and 5745 Å, but neither can be assigned with preferential certainty. Finally, it is relevant to comment that even though Pb(III) (Pb^{2+}) is the formal oxidation state of lead in solid PbO, the ablation plume reveals almost exclusively the presence of only the neutral species, Pb(I). Furthermore, the photoemission peak at 5613 Å corresponds reasonably closely to where PbO(g) is expected to luminesce (5618 Å), but Pb(II) would also emit (5609 Å) in the vicinity of this observed emission (5613 Å). It is interesting that time-of-flight mass spectrometry (TOF-MS) analysis[22] of the laser plume from PZT (not PbO(s)) targets indicated the presence of Pb(I), Pb(II), and PbO for the laser fluence range 0.2–1.3 J/cm^2. While we cannot determine with complete certainty the presence of PbO in our OES experiments (1.1 J/cm^2), Pb(I) and Pb(II) have been optically identified by us with certainty, as described above already.

The behavior of ZrO_2(s) was explored next. The emission spectra from the ablation plume (900 mTorr O_2) are shown in Figure 2. Due to high spectral resolution and the richness of the transition-metal emissions, a large number of nonoverlapping peaks can be concretely assigned, despite the many observed emissions. Moreover, both spectral regions show photoluminescence from an assortment of both atomic and molecular species. Figure 2A displays atomic emissions from Zr(I) and Zr(II), although mainly from intensely emitting Zr(I) (Table 3). In addition, molecular emitters were also observed in the ablation plume from ZrO_2 targets. However, only peaks 8 and 20 are uniquely identifiable among known species as arising from ZrO and O_2 emission, respectively. Several other observed peaks also correspond closely to photoluminescence from more than one possible species, e.g., peak 14 (3732 Å) can result from either or both Zr(II) and O_2. In Figure 2B, Zr(I) and ZrO emission peaks dominate, with a ca. equal amount of each species (Table 4), assuming that both have the same quantum efficiency. However, no uniquely identifiable Zr(II) peak is present (Table 4). Interestingly, the occurrence of the previously observed (i.e., Figure 1) molecular emitter, O_2^+, in the plume from PbO(s) is again seen (5601 and 5851 Å) in the plume from ZrO_2(s). Overall, there are nearly equal distributions of Zr(I) and Zr(II) emission lines observed when considering both recorded spectral regions, whereas

(21) Pearse, R. W. B.; Gaydon, A. G. *The Identification of Molecular Spectra*, 3rd ed.; John Wiley and Sons: New York, 1963.

(22) Leuchtner, R. E.; Horwitz, J. S.; Chrisey, D. B. *Ferroelectric Thin Films II*; Kingon, A. I., Myers, E. R., Tuttle, B., Eds.; Mat. Res. Soc. Proc.; Pittsburgh, PA, 1992; Vol. 243, p 525.

Table 3. Laser Ablation of ZrO_2 (900 mTorr of O_2): Clearly Identifiable Photoluminescence Peaks of Gaseous Atomic and Molecular Species Observed in the "Blue" Region (340–415 nm)

peak no.	emitting species†	experimental wavelengths, Å	lit.‡ wavelengths, Å	lit. ref
1	Zr(II)	3430	3431	20
2	Zr(II)	3436	3438	20
3	Zr(II)[a]	3479	3479,[a] 3481[a]	20
4	Zr(II)[b]/ZrO[c]	3496	3496,[b] 3493[c]	20, 21
5	Zr(II)[d]/ZrO[e]	3506	3506,[d] 3506[e]	20, 21
6	Zr(I)[f]/Zr(II)[g]/$O_2^{+(ii)}$	3521	3520,[f] 3522,[f] 3521,[g] 3518[(ii)]	20, 21
7	Zr(I)[h]/O_2[i]	3543	3543,[h] 3542[i]	20, 21
8	ZrO	3589	3590	21
9	Zr(I)[j]/$O_2^{+(k)}$	3602	3601,[j] 3604[k]	20, 21
10	Zr(II)	3614	3615	20
11	Zr(I)	3663	3664	20
12	Zr(II)[l]/ZrO[m]	3700	3698,[l] 3700[m]	20, 21
13	Zr(II)	3710	3709	20
14	Zr(I)[n]/O_2[p]	3732	3731,[n] 3734[p]	20, 21
15	Zr(II)	3752	3752	20
16	Zr(I)[q]/ZrO_2[r]	3820	3822,[q] 3818[r]	20, 21
17	Zr(I)	3839	3836	20
18	Zr(I)	3865	3864	20
19	Zr(I)[s]/Zr(II)[t]	3918	3922,[s] 3916[t]	20
20	O_2	3937	3938	21
21	Zr(II)	3960	3958	20
22	Zr(II)	3993	3991	20
23	Zr(II)	4001	3999	20
24	Zr(I)[u]/Zr(II)[v]	4020	4021,[u] 4018[v]	20
25	Zr(I)[w]/Zr(II)[x]	4051	4055,[w] 4049[x]	20

† Excited-state neutral atoms are labeled I; excited-state ions (+1) are labeled II. ‡ Emission wavelengths of arc or spark excitations. [a] Zr(II) emits at 3479 and 3481 Å. [b,c] Zr(II) and ZrO emit at 3496 and 3493 Å, respectively. [d,e] Zr(II) and ZrO both emit at 3506 Å. [f,g,(ii)] Zr(I) emits at 3520 and 3522 Å, Zr(II) emits at 3521 Å. O_2^+ emits at 3518 Å. [h,i] Zr(II) and O_2 emit at 3543 and 3542 Å, respectively. [j,k] Zr(I) and O_2^+ emit at 3601 and 3604 Å, respectively. [l,m] Zr(II) and ZrO emit at 3698 and 3700 Å, respectively. [n,p] Zr(II) and O_2 emit at 3731 and 3734 Å, respectively. [q,r] Zr(I) and ZrO emit at 3822 and 3818 Å, respectively. [s,t] Zr(I) and Zr(II) emit at 3922 and 3916 Å, respectively. [u,v] Zr(I) and Zr(II) emit at 4021 and 4018 Å, respectively. [w,x] Zr(I) and Zr(II) emit at 4055 and 4049 Å, respectively.

molecular emissions are more prominent in the 555–630 nm region (Figure 2B). Again, we pointed out that even though Zr(V) (i.e., Zr^{4+}) is the simplistic formal ionic charge of zirconium in ZrO_2(s), we only observe photoemission evidence for low-valence Zr(I) and Zr(II) in the ablation plume from ZrO_2(s). This is further discussed below. Finally, it is also of interest that the TOF-MS spectrum[22] from the ablation plume of PZT showed that Zr(I), Zr(II), ZrO, and ZrO^+ were present. This coincides with our findings, except that we do not observe ZrO^+.

The optical emission spectra of the ablation plume of TiO_2 were measured next and are shown in Figure 3. Again, as in the photoablation of ZrO_2, we note both atomic and molecular emissions. Because of the extremely large number of neutral atomic and ionic Ti emission lines within this wavelength range (340–415 nm), Figure 3A appears quite complex and, in fact, yields relatively fewer uniquely assignable peaks compared to the previously discussed spectra from ZrO_2. However, photoluminescence from O(I), Ti(I), and Ti(II) (Table 5) is observed. Of these Ti(I) and Ti(II) emissions—about an equal number of each—are the only uniquely identifiable atomic lines (Table 5). Atomic O(I) and Ti(I) are together assigned to peak 10 (3823 Å). Only one molecular species, O_2^+ (3521 Å), is unambiguously identified (peak 3). Interestingly, this exact same O_2^+ emission peak was also observed in the ablation plume from ZrO_2 (peak 6) discussed above, with other assignments being Zr(I) and Zr(II). While the spectrum of Figure 3B contains more assignable peaks, almost exclusively it is Ti(I) which is the only atomic species responsible for these emissions (Table 6). Furthermore, Ti(I) is the major light-emitting atomic species observed when surveying both spectral regions (Figure 3A,B). Figure 3B also reveals oxide emission from TiO and TiO_2, the TiO_2 (5892 Å, peak 24) assignment being the only polyatomic emission observed in all the spectra of the present ablation plumes from these oxides. This observation will again be discussed in a section below.

Table 4. Laser Ablation of ZrO_2 (900 mTorr of O_2): Clearly Identifiable Photoluminescence Peaks of Gaseous Atomic and Molecular Species Observed in the "Red" Region (555–630 nm)

peak no.	emitting species†	experimental wavelengths, Å	lit.‡ wavelengths, Å	lit. ref
26	O_2^+	5601	5598	21
27	Zr(I)[a]/ZrO[b]	5623	5620,[a] 5624,[a] 5624[b]	20,21
28	ZrO	5653	5658	21
29	Zr(I)	5665	5665	20
30	Zr(I)	5681	5681	20
31	Zr(I)	5731	5736	20
32	Zr(I)	5795	5798	20
33	ZrO	5806	5809	21
34	O_2^+	5851	5847	21
35	Zr(I)	5879	5880	20
36	Zr(I)[c]	5988	5984,[c] 5985[c]	20
37	Zr(I)[d]/ZrO[e]	6061	6063,[d] 6059[e]	20, 21
38	Zr(II)	6116	6115	20
39	Zr(I)[f]/ZrO[g]	6223	6221,[f] 6223[g]	20, 21
40	Zr(I)[h]/O[i]	6260	6261,[h] 6261[i]	20, 21
41	Zr(I)[j]	6304	6300,[j] 6304[j]	20
42	Zr(I)[k]/Zr(II)[l]/ZrO[m]	6316	6315,[k] 6314,[l] 6318[m]	20, 21

† Excited-state neutral atoms are labeled I; excited-state ions (+1) are labeled II. ‡ Emission wavelengths of arc or spark excitations. [a,b] Zr(I) emits at 5620 and 5624 Å; ZrO emits at 5624 Å. [c] Zr(I) emits at 5984 and 5985 Å. [d,e] Zr(I) and ZrO emit at 6063 and 6059 Å, respectively. [f,g] Zr(I) and ZrO emit at 6221 and 6223 Å, respectively. [h,i] ZrO and O both emit at 6261 Å; the charge of O is unknown. [j] Zr(I) emits at 6300 and 6304 Å. [k,l,m] Zr(I), Zr(II), and ZrO emit at 6315, 6314, and 6318 Å, respectively.

Table 5. Laser Ablation of TiO_2 (900 mTorr of O_2): Clearly Identifiable Photoluminescence Peaks of Gaseous Atomic and Molecular Species Observed in the "Blue" Region (340–415 nm)

peak no.	emitting species†	experimental wavelengths, Å	lit.‡ wavelengths, Å	lit. ref
1	Ti(II)	3461	3462	20
2	Ti(II)	3482	3484	20
3	O_2^+	3521	3518	21
4	Ti(II)	3536	3535	20
5	Ti(I)[a]/$O_2^{+(b)}$	3603	3601,[a] 3604,[a] 3606,[a] 3604[b,f]	20, 21
6	Ti(I)[c]/Ti(II)[d]	3626	3626,[c] 3625[d]	20
7	Ti(I)[e]/Ti(II)[f]	3657	3654,[e] 3658,[e] 3660[f]	20
8	Ti(I)[g]/Ti(II)[h]	3688	3690,[g] 3685[h]	20
9	Ti(I)[i]	3703	3702,[i] 3704[i]	20
10	Ti(I)[j]/O(I)[k]	3823	3822,[j] 3823,[k] 3825[k]	20, 21
11	Ti(I)	3993	3990[a]	20

† Excited-state neutral atoms are labeled I; excited-state ions (+1) are labeled II. ‡ Emission wavelengths of arc or spark excitation. [a,b] Ti(I) emits at 3601, 3604, and 3606 Å; O_2^+ emits at 3604 Å. [c,d] Ti(I) and Ti(II) emit at 3626 and 3625 Å, respectively. [e,f] Ti(I) emits at 3654 and 3658 Å; Ti(II) emits at 3660 Å. [g,h] Ti(I) and Ti(II) emit at 3690 and 3685 Å, respectively. [i] Ti(I) emits at 3702 and 3704 Å. [j,k] Ti(I) emits at 3822 Å; O(I) emits at 3823 and 3825 Å.

Table 6. Laser Ablation of TiO_2 (900 mTorr of O_2): Clearly Identifiable Photoluminescence Peaks of Gaseous Atomic and Molecular Species Observed in the "Red" Region (555–630 nm)

peak no.	emitting species†	experimental wavelengths, Å	lit.‡ wavelengths, Å	lit. ref
12	TiO	5602	5604	21
13	Ti(I)	5642	5644	20
14	Ti(I)[a]/TiO[b]	5659	5662,[a] 5663,[a] 5662[b]	20, 21
15	Ti(I)[c]/TiO[d]	5671	5675,[c] 5668[d]	20, 21
16	Ti(I)	5685	5689	20
17	TiO[e]	5698	5694,[e] 5701[e]	21
18	Ti(I)[f]	5709	5708,[f] 5712[f]	20
19	TiO	5733	5733	21
20	Ti(I)[g]	5766	5763,[g] 5766[g]	20
21	Ti(I)	5797	5797	20
22	Ti(I)[h]/TiO[i]/O_2^+ [(j)]	5817	5814,[h] 5815,[i] 5814[j]	20, 21
23	TiO	5859	5862	21
24	TiO_2[s]	5892	5894	23
25	Ti(I)	5937	5938	20
26	Ti(I)[k]/O(I)[l]	5950	5953,[k] 5951[l]	20, 21
27	Ti(I)	5964	5966	20
28	Ti(I)	5978	5979	20
29	Ti(I)	6001	6000	20
30	Ti(I)	6103	6099	20
31	Ti(I)	6130	6126	20
32	Ti(I)[m]/TiO[n]	6149	6146,[m] 6150,[m] 6149[n]	20, 21
33	TiO	6166	6162	21
34	TiO[p]	6179	6175,[p] 6184[p]	21
35	Ti(I)	6253	6258	20
36	Ti(I)[q]/TiO[r]	6275	6273,[q] 6278,[q] 6276[r]	20, 21

† Excited-state neutral atoms are labeled I; excited-state ions (+1) are labeled II. ‡ Emission wavelengths of arc or spark excitations. [a,b] Ti(I) emits at 5662 and 5663 Å; TiO emits at 5662 Å. [c,d] Ti(I) and TiO emit at 5675 and 5668 Å, respectively. [e] TiO emits at 5694 and 5701 Å. [f] Ti(I) emits at 5708 and 5712 Å. [g] Ti(I) emits at 5763 and 5766 Å. [h,i,j] Ti(I), TiO, and O_2^+ emit at 5814, 5815, and 5814 Å, respectively. [k,l] Ti(I) and O(I) emit at 5853 and 5951 Å, respectively. [m,n] Ti(I) emits at 6146 and 6150 Å; TiO emits at 6149 Å. [p] TiO emits at 6175 and 6184 Å. [q,r] Ti(I) emits at 6273 and 6278 Å; TiO emits at 6276 Å. [s] This corresponds to the 100 → 300 emission (23); also see Results and Discussion of this paper.

Other peaks such as number 22 (5817 Å) are assigned to one or more of Ti(I), TiO, and O_2^+ species, and peak 26 (5950 Å) results from one or both Ti(I) and O(I) emissions. We again point out that for this oxide, ZrO_2, that despite the Ti(V) formal ionic charge, we only observe emissions from the low-valent Ti(I) and Ti(II). It is an interesting comparison to note that the TOF-MS spectrum[22] of the laser plume from PZT (not TiO_2) also revealed the presence of Ti(I) and Ti(II) but also of molecular TiO. While our OES data also demonstrated the presence of these three, we also observe the TiO_2(g) emission which has not observed in that study.[22]

Following the above-described results for the components of PZT, we now discuss the emission spectra of the plume from bulk PZT (Figure 4). The data summarized in Tables 7 and 8 demonstrate that there is an abundance of clearly assignable emission peaks, most but not all of which were observed and discussed above in the spectra of ablation plumes from PbO, ZrO_2, and TiO_2 targets. Figure 4A shows both atomic and molecular emissions. Atomic emission lines which are uniquely identifiable include those of Pb(I), Zr(I), Zr-(II), Ti(II), and O(II), with the Zr emission lines being most abundant (Table 7). Molecular emissions corresponding to ZrO and O_2 are also present but are confirmable by fewer lines. In addition there are also many other peaks, but which are assignable only to two or more species. Figure 4B and Table 8 also reveal the presence of neutral atomic but also molecular emitters. From this spectrum peaks resulting from neutral atomic species are unambiguously assignable to Pb(I), Zr(I), and Ti(I), with emissions from Ti(I) being most abundant (Table 8). The Pb(II) emission at 6010 Å (peak 57) is the only ionized monoatomic peak seen here. Peaks arising from molecular emissions are uniquely assignable in this spectrum to each of the diatomic oxides (PbO, ZrO, and TiO), but O_2^+ and the polyatomic TiO_2 are also identified here (and were seen in the plume from the TiO_2 ablation described above). While each of these peaks belongs to just one species, Figure 4A and Table 7 also make clear that many additional peaks can potentially correspond to more than one emitting species. For ablated PZT it is also of interest to compare our list of photoemission-detected species with the list of those detected by TOF-MS (from laser ablation of PZT).[22] In that study Pb(I), Pb(II), Zr(I), Zr-(II), Ti(I), Ti(II), PbO, ZrO^+, ZrO, and TiO were found, for the laser fluence range 0.2–1.3 J/cm^2. In our present study using the 1.1 J/cm^2 laser fluence, all of these except ZrO^+ are also detected by us using OES. Additionally, we find that other photoexcited species are strongly suggested to be present, i.e., TiO_2, O_2, O_2^+, O(I), and O(II) (Figure 4A,B, Tables 7 and 8).

Regarding our consistent observation of O_2^+ and our occasional observation of O_2, O(I), and O(II) in the plasma plumes from the metal oxides and PZT in 900 mTorr of O_2, as well as in the plumes under vacuum conditions (not presented), we suggest that the occurrence of these species may be attributable to one or both of the following origins: (1) at our 10^{-6} Torr working vacuum pressure, lingering traces of ambient O_2(g) and/or H_2O(g) are potential sources of the oxygen species, which become photoemissive upon laser ablation; (2) it is well established that the crystal lattices such as our metal oxide and PZT targets are, as expected, very rich sources of oxygen, which upon laser irradiation may also lead to the observed oxygen species via gas-phase processes.

An additional comment is needed regarding the photoluminescence evidence for the presence of polyatomic TiO_2(g) in the ablation plumes from TiO_2 and PZT targets. For the photoluminescence ranges measured at present, we assigned the weak 5892 and 5895 Å lines from plumes derived from TiO_2(s) and PZT(s), respectively, to the expected 5894 Å vibronic (100 → 300) emission[23] of TiO_2(g). However, we could not additionally confirm this because the present measurement ranges did not allow for the detection of the most intense emission[23] expected at 5288.6 Å (000 → 000). Had this purely electronic emission been observed along with our observed 5892 Å and 5895 Å lines, we would have been able to establish even more firmly the occurrence of gaseous TiO_2(g) in the ablation plumes from TiO_2 and PZT targets.

It is of some interest to ponder possible reasons for the presence of the lower-charged metal species, M(I) and M(II), rather than the higher-charged species such as Pb(III), Zr(V), and Ti(V), i.e., Pb^{2+}, Zr^{4+}, and Ti^{4+}, respectively. The first factor to take into account is that

(23) DeVore, T. C. *High Temp. Sci.* **1982**, *15*, 219.

Table 7. Laser Ablation of $PbZr_xTi_{1-x}O_3$ (900 mTorr of O_2): Clearly Identifiable Photoluminescence Peaks of Gaseous Atomic and Molecular Species Observed in the "Blue" Region (340–415 nm)

peak no.	emitting species[†,a]	experimental wavelengths, Å	peak no.	emitting species[†,a]	experimental wavelengths, Å
1	Zr(II)	3430	17	Zr(II)	3711
2	Zr(II)	3436	18	Zr(II)/O_2	3732
3	Zr(II)/ZrO/Ti(II)	3479	19	Pb(I)	3743
4	Zr(II)/ZrO	3496	20	Zr(II)	3754
5	Zr(II)/ZrO	3506	21	Ti(II)[b]	3761
6	Zr(I)/Zr(II)/O_2^+	3521	22	Zr(I)	3839
7	Ti(II)	3536	23	Zr(I)	3865
8	Zr(II)/O_2	3543	24	O(II)[b]	3885
9	Pb(I)	3574	25	Zr(II)	3915
10	ZrO	3589	26	O_2	3937
11	Zr(I)/Ti(I)/O_2^+	3602	27	Zr(II)	3960
12	Zr(II)	3614	28	ZrO[b]	3984
13	Zr(I)/Ti(II)	3662	29	Zr(II)/Ti(I)	3993
14	Pb(I)	3674	30	Zr(II)	4001
15	Ti(I)/Ti(II)	3687	31	Zr(II)	4049
16	Zr(II)/ZrO/Ti(I)	3700	32	Pb(I)	4059

[†] Excited-state neutral atoms are labeled I; excited-state ions (+1) are labeled II. [a] Species identified in OES of PbO, ZrO_2, and/or TiO_2. [b] Species not clearly identified in OES of PbO, ZrO_2, and/or TiO_2, or appearing for the first time.

Table 8. Laser Ablation of $PbZr_xTi_{1-x}O_3$ (900 mTorr of O_2): Clearly Identifiable Photoluminescence Peaks of Gaseous Atomic and Molecular Species Observed in the "Red" Regions (555–630 nm)

peak no.	emitting species[†,a]	experimental wavelengths, Å	peak no.	emitting species[†,a]	experimental wavelengths, Å
33	TiO[b]/O_2^+	5597	51	Ti(I)	5937
34	PbO	5614	52	O(I)[b]	5959
35	Zr(I)/ZrO	5626	53	Ti(I)	5968
36	Ti(I)	5646	54	$O_2^{+\,(b)}$	5973
37	ZrO	5655	55	Zr(I)	5985
38	Zr(I)/Ti(I)/TiO	5666	56	Pb(I)[b]	6005
39	Ti(I)	5674	57	Pb(II)	6010
40	Zr(I)	5681	58	ZrO[b]	6071
41	TiO	5701	59	Ti(I)	6096
42	Zr(I)/TiO	5734	60	Ti(I)/TiO	6149
43	Ti(I)	5765	61	Pb[b,c]/ZrO[b]	6169
44	Zr(I)	5795	62	TiO[b]	6189
45	ZrO/Ti(I)[b]	5806	63	ZrO[b]	6228
46	O_2^+	5852	64	PbO[b]	6252
47	Ti(I)/TiO	5865	65	Ti(I)[b]/ZrO/O[c]	6260
48	Zr(I)	5877	66	Zr(I)[b]	6282
49	$O_2^{+\,(b)}$	5889	67	Zr(I)	6306
50	TiO_2[d]	5895			

[†] Excited-state neutral atoms are labeled I; excited-state ions (+1) are labeled (II). [a] Species identified in OES of PbO, ZrO_2, and/or TiO_2. [b] Species not clearly identified in OES of PbO, ZrO_2, and/or TiO_2, or appearing for the first time. [c] The charge of the species is unknown. [d] This corresponds to the 100 → 300 emission (23); see also Results and Discussion of this paper.

the simplistic formal ionic charges, such as 4+ of Ti^{4+} etc., probably do not reflect the real electron density distribution in the Ti–O bonds of the octahedrally coordinated {TiO_6} moiety within TiO_2(s) as well as in other compounds in which a metal is surrounded by n oxygens or other "ligands". Instead of formal ionic charges being real, e.g., the formal Ti^{4+}–O^{2-} charges in TiO_2(s), the ions are probably closer to neutrality, e.g., $Ti^{\delta+}$–$O^{\delta-}$, with $|\delta| \leq$ |formal ionic charge|. This should come as no surprise, since formal ionic charges are assigned artificially by assuming 100% ionicity (complete transfer of electrons) and, therefore, are assumed to contain zero covalency (no sharing of electron density by atomic orbital overlap). Obviously, this formalism represents an unreal scenario, for even in the extreme type polar (ionic) alkali halides, e.g., CsF, quantum mechanical calculations have clearly shown[24] that there is, in fact, not a complete charge transfer, i.e., there is some electron sharing. As another example, the results of a sound theoretically-based charge density analysis[25]—as derived from the self-consistent-charge Xα (SCC-Xα) method—of the trigonal bipyramidal VF_5 molecule indicate that the effective charges on V, F(axial), and F (equatorial) are +1.67, −0.34, and −0.33, respectively, not the formal ionic charges of +5 for V and −1 for each F. Yet another source of new light on this subject is the result of electron-density distribution analysis[26] of data observed by very accurate X-ray diffraction, which allows one to experimentally estimate net charges on "atoms", such as in transition-metal complexes. Two methods of approximation are often employed for these determinations, a direct integration (DI) method and an extended L-shell (ELS) method, both yielding different but directionally similar results. For example, in tetrahedrally coordinated CrO_4^{2-} with Cr assigned the +6 formal oxidation state, the DI and ELS methods yield, respectively, +0.1 and +2.78 for the net atomic charge on chromium.[26] These values, which

(24) Grodzicki, M. In: Maksic, Z. B., Ed.; *Theoretical Models of Chemical Bonding (Part 2)*; Springer-Verlag: Berlin, 1990; p 440.

(25) Grodzicki, M.; Elbel, S. In: Maksic, Z. B., Ed.; *Molecular Structure and Bonding*; Ellis Horwood: Chichester, 1987; p 239.

(26) Toriumi, K.; Saito, Y.; In: Emeléus, H. J., Sharpe, A. G., Eds.; *Advances in Inorganic Chemistry and Radiochemistry*; Academic Press: New York, 1983; Vol. 23, pp 27–81.

certainly are not the same, are obviously significantly less than the assigned formal ionic charge of +6. Likewise, in octahedrally coordinated $[Co(NH_3)_6]^{3+}$, where Co is formally Co^{+3}, the DI and ELS methods give net atomic charges of +0.7 and +0.8, respectively, for Co.[26] In conclusion, what suggests itself is that finding the low-charged atomic metal species, e.g., $Ti^{0,+}$, rather than the high formal ionically charged species, e.g, Ti^{4+}, may be a consequence of low-valent species already being present within the solid target even prior to laser impact.

A second factor of probable relevance as to why we observe these low-charge metal species is that ionization enthalpies of elements rise dramatically after the first ionization. For example, for Ti the first through fifth ionization energies are 6.82, 13.56, 27.49, 43.27, and 99.22 eV, respectively, i.e., the energy requirement roughly doubles for each subsequent ionization. Therefore, if the Ti in TiO_2(s) were other than ca. +1, the ca. 5 eV laser energy per photon could not bring about the ionizations to higher charges such as $Ti^{2+,3+,4+}$. A potential two-photon absorption/ionization of a hypothetical (but unlikely) Ti^0 in TiO_2(s) getting ionized to Ti^+ is possible if a two-photon laser absorption mechanism, $2h\nu$ (2 × 5 eV), were responsible for exciting the $\{TiO_6\}^Q$ (A) moiety getting converted to $\{Ti^+(O_6)^-\}^Q$ (B), i.e., a transition from the electronic ground state of the former (A) to a 10 eV excited vibronic level of the latter (B).

There is a third potential cause for not observing higher-charged metal ions, and this may be due to gas-phase partial charge neutralizations taking place. Even if higher-charged species (higher than 0 and +1) were ejected from the target, it is possible that such species are rapidly reduced to lower positive charge states by electron attachment within the plasma created by the laser. For example, we consider it possible to estimate whether the laser radiation energy (2480 Å, 5.0 eV) is sufficiently energetic to potentially bring about a conversion (intramolecular metal−ion reduction) such as $Pb^{2+} \rightarrow Pb^+$ by the oxo ligand (O^{Q-})-to-metal (Pb^{2+}) charge transfer. We visualize such an "intramolecular" electron-transfer process within the oxides, such as $O^{Q-} \rightarrow Pb^{Q+}$, to be induced, resulting in $Pb^{+Q-1}-O^{-(Q+1)}$ when the laser radiation interacts with the solid and just before ablation takes place. For the quantitative estimate of the photon energy required for such a process, we use Jorgensen's optical electronegativities (χ^0) for metals and their ligands (e.g., O^{2-}, etc.). These values were empirically derived for metals and ligands "bearing" their normal formal ionic charges, regardless of what real charges are present within the ML_n moieties such as our PbO, ZrO_2, and TiO_2. When normally using the Jorgensen equation, one can predict with established accuracy the lowest energy electron charge transfer transition for ligand-to-metal ($O^{2-} \rightarrow Pb^{2+}$), LMCT, or metal-to-ligand ($O^{2-} \leftarrow Pb^{2+}$), MLCT, charge-transfer energies. One needs to use the Jorgensen optical electronegativities (χ^0)[27] for species under present consideration, viz., 1.6, 2.1, and 1.0 (est.) for, respectively, Zr(V)(d^0), Ti(V)(d^0), and Pb(III)($d^{10}s^2$) in octahedral environments, and $\chi^0(O^{2-})$ is 3.2 for its pπ electrons. We obtained χ^0[Pb(III)] by using data known for $[PbCl_6]^{4-}$: $\nu_{CT} > 50\,000$ cm^{-1} (we used 60 000 cm^{-1}) and $\chi^0(Cl^-) = 3.0$. In this way one obtains χ^0[Pb(III)] = 1.0 from Jorgensen's equation,[27] i.e., $\nu_{CT}[Cl^- \rightarrow Pb(III)] = 30\,000\{\chi^0[Cl^-] - \chi^0[Pb(III)]\}$ in cm^{-1} units. Therefore, the lowest energy $O^{2-} \rightarrow M^{n+}$ CT band is predicted at 34 500 cm^{-1} (4.28 eV), 48 000 cm^{-1} (5.95 eV), and 66 000 cm^{-1} (8.18 eV), respectively, for TiO_2, ZrO_2, and PbO. It follows that because of the laser radiation's 5.0 eV/photon (248 nm or 40 320 cm^{-1}), such a charge neutralization can, in principle, be effected by a one-photon process in only TiO_2(s). However, because the peak power of our pulses is ca. 7×10^6 W (pulse width 25 ns at half-height and laser energy of 0.20 J/pulse), some $O^{2-} \rightarrow M^{n+}$ charge-transfer processes can, in principle, take place by two-photon absorption even for ZrO_2 and PbO. Such processes may, therefore, contribute toward the appearance of optically observed low-charge metal species $M^{0,+}$. Finally, low-valent $M^{0,+}$ species might also get generated from higher-charged ones in the observed plasma, which likely consists of $\{e^-, M^{n+}, O_2^+, O_2, O, ...\}$, thereby resulting in the reduction of coulombically favored higher-charged metal ions by plasma electrons.

Another metal oxide solid-state parameter of interest is the atomization enthalpy, ΔH°_a, for forming (neutral) atoms. ΔH°_a values are of interest because the solids PbO, ZrO_2, and TiO_2 yield, as expected, dominantly neutral atoms in the plume. In fact, ΔH°_a values are 158, 524, and 466 kcal/mol for the solids PbO, ZrO_2, and TiO_2, respectively. These numbers are consistent with finding almost exclusively neutral atoms in the photoemission spectra of PbO, whereas gaseous, molecular metal oxide species, i.e., TiO, TiO_2, and ZrO, are observable in the plumes from ZrO_2 and TiO_2 targets.

The laser ablation process in laser ablation deposition of multicomponent oxides probably involves a complex combination of various particle ejection mechanisms. It has been hypothesized[28] that three main particle-ejection mechanisms may be involved, namely, (i) ablation (particle ejection induced by shock waves created in the solid target during laser impact at the center of the irradiated area), (ii) sputtering (produced by bombardment of the target by ions from the plasma created in front of the target and dominant at the periphery of the laser-impacted area), and (iii) evaporation (due to target heating by laser impact). This three-component hypothesis is based on two kinds of experimental data: (a) measurements of the energy distribution of particles ejected by PZT targets ablated by excimer lasers,[22] which show three energy distributions with peaks at about 1 eV (characteristic of the evaporation process), 5−10 eV (characteristic of the sputtering process), and ≥30 eV (characteristic of the shock wave-induced ablation process) and (b) studies of surface topography of the laser-impacted area[28] which reveal the presence of conical features (due to a growth process induced by the ablation mechanism at the center of the ablated area) and cones (characteristic of a sputtering process on the periphery of the laser-impacted area, where sputtering produced by plasma ions may be dominant over the laser ablation process). Further details about the particle ejection mechanisms discussed above can be found elsewhere.[28]

(27) Jorgensen, C. K. *Oxidation Numbers and Oxidation States*; Springer-Verlag: New York, 1969; pp 146−147.

(28) Auciello, O., in preparation.

It is not clear at the moment what the relative influence is of neutral and charged atomic and molecular oxide species on the composition, microstructure, and properties of PZT films, but film growth is not the subject of this publication. However, by extension of what was found in the past for the case of the synthesis of high-temperature superconducting thin films,[11,29] we can speculate that the presence of oxide species in the plume may contribute to producing stoichiometric films induced by appropriate rates of arrival of metallic and oxygen atoms at the surface. In addition, a balanced rate of arrival of separated metal and oxygen atoms at the surface may also contribute to producing stoichiometric films. Obviously, the next step in the line of investigation initiated with this paper is to try to quantify the relative rate of arrival of metallic and oxygen atoms and oxide molecules at the substrate surface. An important point to be considered is that as we increase the oxygen pressure during ablation of PZT and the component metal oxide targets, from below the mTorr range to 900 mTorr (the pressure used for the data reported in this paper), the relative abundance of all metal oxide molecules observed increases, as revealed by the increase in the peak intensities. This indicates that perhaps the reaction of metal and oxygen atoms in the gas phase increases as the mean free path for collision processes decreases with increasing pressure. One may mistakenly assume then, that a 900 mTorr of oxygen background pressure would be desirable over lower pressures during film deposition to maximize the formation of metal oxide molecules. However, other parameters very relevant to film deposition need to be considered. We have recently demonstrated[30] that for oxygen pressures above 300 mTorr, the ablated plume from PZT targets is highly focused, such that the angular distribution of ablated species follows a $\cos^n\theta$ law. This is an undesirable condition if one wants to scale the PLAD technique to generate uniform films over large substrate areas. In addition, at such relatively high pressures, the energetic species (20−100 eV)[29] produced during the ablation process are fully thermalized due to gas collision processes. Therefore, one of the advantages of the PLAD technique is lost, i.e., the ability of producing stoichiometric films with appropriate crystallinity at relatively low substrate temperature.

Currently, PZT films are deposited in our lab in oxygen background pressures reduced to about 300 mTorr. Under this condition we have observed increased emission intensity from metal oxide (MO_n) molecules compared to the ablation from PZT in vacuum. Further work is necessary to quantify the effect of oxygen pressure on the intensity of oxide species in the plume.

CM940297Y

(29) Cheung, J.; Horwitz, J. *Pulsed Laser Deposition*; Special Issue of the MRS Bulletin, **1992**, *17*, 30.

(30) Lichtenwalner, D. J.; Auciello, O.; Dat, R.; Kingon, A. I. *J. Appl. Phys.* **1993**, *74*(12), 7497.